Spectrally Silent Transitions in the Bacteriorhodopsin Photocycle

I. Chizhov,* D. S. Chernavskii,# M. Engelhard,* K.-H. Mueller,* B. V. Zubov,§ and B. Hess*
*Max-Planck-Institut für Molekulare Physiologie, 44139 Dortmund, Germany, and #P. N. Lebedev Physical Institute and §General Physics Institute of the Russian Academy of Sciences, 117942 Moscow, Russia

ABSTRACT The photocycle kinetics of bacteriorhodopsin were analyzed from 0 to 40°C at 101 wavelengths (330–730 nm). The data can be satisfactorily approximated by eight exponents. The slowest component (half-time 20 ms at 20°C) belongs to the 13-*cis* cycle. The residual seven exponentials that are sufficient to describe the all-*trans* photocycle indicate that at least seven intermediates of the all-*trans* cycle must exist, although only five spectrally distinct species (K, L, M, N, and O) have been identified. These seven exponentials and their spectra at different temperatures provide the basis for the discussion of various kinetic schemes of the relaxation. The simplest model of irreversible sequential transitions includes after the first K → L step the quasiequilibria of L↔M, M↔N, and N↔O intermediates. These quasiequilibria are controlled by rate-limiting dynamics of the protein and/or proton transfer steps outside the chromophore region. Thus there exists an apparent kinetic paradox (i.e., why is the number of exponents of relaxation (at least seven) higher than the number of distinct spectral intermediates (only five)), which can be explained by assuming that some of the transitions correspond to changes in the quasiequilibria between spectrally distinct intermediates (i.e., are spectrally silent).

INTRODUCTION

The membrane protein bacteriorhodopsin (bR) from *Halobacterium salinarium* is a well-studied member of the family of photoactive retinal-containing proteins. It functions as a light-driven proton pump that transfers a proton across the cytoplasmic membrane. Its retinal chromophore is covalently bound via a protonated Schiff base (SB) (for a review see Lanyi, 1993). Under continuous illumination this process establishes a transmembrane electrochemical gradient $\Delta\mu_{H+}$, which the bacterial cell uses as an energy source. The single cycle of proton pumping is characterized by a complex series of thermally activated transitions of the bR with half-times from picoseconds to several milliseconds at room temperature. These transitions had initially been detected in the transient absorption kinetics (Lozier et al., 1975; Chu Kung et al., 1975). Similar relaxation components were later found in the time-resolved ultraviolet and infrared as well as electrochemical measurements (e.g., Müller et al., 1991). The principal intermediates originally identified by their visible spectral features as K_{610}, L_{550}, M_{412}, N_{550}, and O_{640} (Lozier et al., 1975) have been associated with intramolecular changes such as protonation-deprotonation of the protein (Chance et al., 1975), and later of the SB, Asp85 and 96, the isomerization of retinal, and general conformational transitions of the protein (see review Birge, 1990). However, the problem of deriving a complete description of the photocycle from apparent kinetic components is still unsolved.

The simplest model of a sequence of irreversible transitions K → L → M → N → O → bR (Lozier et al., 1975) with an order of increasing half-times could not fully describe the experimental data. The first indication of problems with this scheme was the unusual temperature dependence of the transient concentration of the O intermediate. Whereas the ratio of the half-times of formation and decay of O is almost temperature independent, the transient concentration of this intermediate increases significantly with temperature. As a solution to this problem, a branching of the photocycle at earlier stages was proposed (Sherman et al., 1976). An increase in accuracy of transient absorption data and multiexponential analysis revealed more components than predicted by the above scheme. For example, the two-exponential decay of the M intermediate has been interpreted as an indication of either two parallel photocycles or a single branched photocycle with two spectrally identical but kinetically distinct M intermediates (Korenstein et al., 1978). Subsequently, the introduction of back-reaction from O to M (Parodi et al., 1984) showed another possible explanation for this kinetic feature (at that time the barely observable N intermediate has mainly been ignored). Temperature jump experiments provided direct evidence for a quasiequilibrium between N and O intermediates (Chernavskii et al., 1989). A similar equilibrium between N and M was demonstrated by a double-pulse excitation method (Druckmann et al., 1993).

These data led to a model of the photocycle that contains after the M intermediate at least two reversible transitions, namely K → L → M ↔ N ↔ O → bR. Theoretically, this photocycle model would account for only five apparent exponentials. If a second M is assumed (e.g., Zimanyi et al., 1992), an additional rate constant totaling six exponentials should be found. However, in the literature more than these six exponentials have been reported, indicating additional intermediates that have not yet been identified spectroscopically. A slow component (~30 ms) was described by Gillbro (1978) and Xie et al. (1987). Furthermore, two fast

Received for publication 12 March 1996 and in final form 18 July 1996.
Address reprint requests to Dr. I. Chizhov, Max-Planck-Institut für Molecular Physiologie, Rheinlanddamm 201, 44139 Dortmund, Germany. Tel.: 49-231-1206-293; Fax: 49-231-1206-389; E-mail: chizhov@mpi-dortmund.mpg.de.

0006-3495/96/11/2329/17 $2.00

components of the M formation (~20 and ~70 μs; Xie et al., 1987) have been identified, totaling seven exponents for a description of the bR photocycle. These seven rates are in contrast to current models of the bR photocycle, in which only six intermediates are contained (Váró and Lanyi, 1991b). There are several papers in which the M rise kinetics were resolved into the three components (e.g. Heberle et al., 1993; Cao et al., 1995; Alexiev et al., 1995). In principle, six intermediates could give rise to a maximum of six apparent rate constants. On the other hand, seven exponentials as found by Xie et al. (1987) correspond to at least seven intermediate states. These discrepancies have not been discussed in later work on the mechanism of the bR photocycle.

In this report we describe the analysis of the photocycle of bR over the whole time range covering the early intermediate K as well as the regeneration of the ground states. Furthermore, the transient absorption kinetics of the photocycle were measured with a high spectral resolution (101 wavelengths from 330 to 730 nm)and a high accuracy of differential amplitudes (max S/N ≈ 400 at 570 nm) in a temperature range of 0–40°C. The results of a multiexponential global fit of the data indicate that there are at least eight exponential components necessary to describe the photocycle satisfactorily. The slowest component, with a half-time of 30 ms, was identified to belong to the 13-*cis* retinal photocycle. This provides seven components, one more than the generally accepted number of intermediates K, L, M1, M2, N, and O. To resolve this discrepancy, a sequential irreversible scheme of the photocycle is analyzed. The sequential irreversible scheme of the photocycle yields a simple coupling between apparent and intrinsic relaxation coefficients and, therefore, is not constrained by the free parameter problem. The model, accounting for all seven apparent transitions, gives only five spectrally distinct intermediates K, L, M, N, and O and shows that at least three apparent rate constants are spectrally silent, which indicates faster equilibrating changes of the balance between spectrally distinct states.

MATERIALS AND METHODS

Sample

The purple membrane suspension was prepared from *Halobacterium salinarium* (strain S9) according to the method of Oesterhelt and Stoeckenius (1974). The bR concentration was 1.8×10^{-4} M, pH 7.2 (0.125 M phosphate buffer). The home-made quartz cuvette (4-mm diameter, 0.4-mm thickness of internal volume) was placed in the vacuumed chamber and in contact with an electrical thermostat (Peltie element, 80 W). The temperature of the sample could be varied from −25 to +80°C and maintained with an accuracy of 0.1°. The cuvette could be refilled through microtubes connected to the sample reservoir.

Measurements

Transient transmission data were acquired with a computer-controlled experimental setup with three digital oscilloscopes (C9-8, USSR, 20-MHz, 8-bit, 2000 points, GPIB interface), and a frequency-doubled Nd-YAG laser (ILTI-405E, USSR; 10 ns, 532 nm, 2 mJ/cm^2). The CAMAC system contained the monochromator's stepping controller, temperature controller, and several modules for time synchronization and laser energy measurement. The acquisition program was homemade.

The optical geometry was as follows. Unfiltered white continuous light from a halogen lamp (only SZS-23 IR-cutoff filter; LOMO, St. Petersburg) was passed through the sample cuvette and reflected at the aluminated rear quartz plate at an angle of 60° to the cuvette plane. After leaving the cuvette the beam was focused on the input slit of a monochromator (MDR-4; LOMO). The laser beam was perpendicular to the cuvette plane. The transmission signal at a selected wavelength was detected by photomultiplier (FEU-100, USSR) equipped with a home made preamplifier. The response time (0.1 μs) and linearity range have been checked before measurements. The actinic pulses had a Gaussian distribution of intensity in the beam, which overlapped the diameter of the cuvette (4 mm) and monitoring beam (3 mm). The signal from the photomultiplier was stored in three digital oscilloscopes with three linear time windows overlapping the transient kinetics from 1 μs to the full completion of the photocycle.

The absorption changes were measured at 11 temperatures (from 0 to 40°C in 4° steps), and at each temperature the transient transmission curves were sampled at 101 wavelengths (from 330 to 730 nm in 4-nm steps). The wavelength was automatically scanned with a computer-controlled step motor. The light adaptation of the sample was provided by a series of 200 saturating laser pulses (5 Hz) at the beginning of wavelength scanning. The ground spectra at each temperature were determined under the same experimental conditions as for kinetic studies, e.g., with the same continuous monitoring of light intensity. Special care was taken to prevent the photosteady accumulation of the long-lived intermediates by the monitoring light; the light intensity was gradually decreased as the sample temperature was reduced, until no detectable changes of ground spectra were seen. The ground spectra of bR were recorded before and after full wavelength scanning to control the light adaptation, the nondisturbing monitoring light intensity, and the probable photodestruction of the sample by actinic pulses. To prevent irreversible photobleaching of the sample (Chizhov et al., 1992b), the measuring cell was continuously refilled with fresh sample during the wavelength scanning at a rate of about 0.1 cell volume per wavelength. At each wavelength 25 laser pulses were used to improve the S/N ratio. Therefore during data acquisition each refreshed sample was illuminated by about 250 laser pulses. After data evaluation we found that under these experimental conditions our transient kinetics also contained the 13-*cis* cycle of about 5–10% of all cycling molecules. This conclusion is based on a comparison of rate constant and amplitude spectrum of the slowest component of transient kinetics from our data with the analysis of Hofrichter et al. (1989) of light- and dark-adapted bR photocycles (see Results).

Computational methods

The transient bR kinetics were measured at 101 different wavelengths with three different overlapping time windows. The analog filtering applied to the data was different for each time window, and thus each has different noise. The average data error is estimated independently for each wavelength and time window from the pretrigger baseline. In addition, data were reduced to a log time scale using a software technique similar to the hardware averaging technique described by Müller and Plesser (1991). Data weights were chosen to give an expected value of the standard deviation of residuals of 1. Estimators for the standard deviation of errors for the optimal solutions were slightly larger than 1 (e.g., see Fig. 3). This is due to an underestimation of the data error of the averaged data, especially at the largest transient increase of transmission (around 570 nm), where the noise level becomes higher than that of the baseline. For details of data weighting see Müller et al., (1991) and Müller and Plesser (1991). The MEXFIT program (Müller et al., 1991) was modified, because each time window must be fitted with a separate baseline.

The following procedure was used for data analysis. The MEXFIT program, which simultaneously finds a single set of exponential functions using the nonlinear least-squares method, was applied independently to the

spectral kinetics (including all 101 wavelengths) at each temperature. Approximations of up to nine exponential terms were tested. The data evaluations at each temperature started with four or five exponential terms, using rates well established in the literature. The standard deviation of errors estimated from the fit, the rate correlation matrix, and the surface of weighted residuals was taken as the criterion for the quality of the obtained fit. In the next step an additional half-time was added. If the estimated standard deviation of errors was reduced, and no degeneration of the fit (detectable by strong correlations in the half-times) occurred, the result was accepted. When the computation failed to give better results, the additional half-time was removed and a new computation was performed with a half-time estimator placed at another position. The procedure was repeated as long as the fit gave better results, or if any possible position for the initial half-time (before, within, and after the half-times found so far) could be achieved. These computations resulted in a set of apparent half-times and their amplitude spectra.

In addition, the Singular Value Decomposition method was used (see Appendix). Furthermore, to discriminate between the meaningful physical components, the temperature behavior of the apparent half-times and the shape and temperature evolution of amplitude spectra were analyzed.

RESULTS

Multiexponential global analysis

Examples of the reduced initial experimental data sets are shown in Fig. 1 as three-dimensional representations depicting log-time, wavelength, and differential amplitudes over a large temperature range. Small, nonsystematic variations in some amplitudes have been found to be due to the instability of laser excitation pulses; however, this instability does not exceed 10% and affects the amplitude accuracy of the derived spectra of intermediates rather than the correspondent rate constants, which were determined with much higher accuracy. In the temperature range from 0°C to 40°C, no significant alterations of transient features of the photocycle, such as a maximum absorbency increase in the blue range (the M intermediate) or a decrease at 570 nm (the bR depletion), were found. The O intermediate can be detected by the increase in induced transient absorbence in the red spectral range. At 0°C the kinetically separated L intermediate and the partially spectrally and kinetically resolved K intermediate can be seen.

An example of wavelength-to-time surfaces of weighted residuals from five to nine exponential data fits at 8°C is given in Fig. 2. Here systematic deviations are seen for five, six, and seven exponential fits. Eight exponents provide the best fit of data without any visible systematic deviation of residuals. The addition of a ninth component to the fit gives the same random distribution of residuals as for eight exponents and, depending on the initial value, the final half-time was very close to the nearest component of the eight-exponential fit. The derived amplitude spectra of these two near-degenerative half-times were unrealistic.

The dependence of the standard deviation (SD) of weighted residuals on the number of applied kinetic components at 8°C is plotted in Fig. 3. Similar curves are obtained at the other temperatures. At temperatures higher than 24°C only seven exponentials are needed to describe the data because the decay of the K intermediate becomes too fast to be measured at the experimental time resolution.

Temperature dependence of rate constants

The Arrhenius plots of apparent rate constants (Fig. 4) also point to the necessity for eight components: the eight-exponent approximation has the smoothest temperature dependence of rate constants (half-times) without significant break points. (In Figs. 4–6 we give the plots of the conventional rate constant versus reciprocal temperature, which represents an estimation of the apparent thermodynamic parameters and the grid lines correspond to the right (half-times) and top (Celsius degrees) axes. The half-time is $t = \ln 2/k$, where k is the rate constant. We discuss all results in terms of half-times and Celsius degrees rather than the correspondent reciprocal values.) As seen in Fig. 4, in the time domain of tens of microseconds and from 24°C to 0°C the noisiest component of the seven-exponent fit (filled circles) splits into two smooth components in the eight-exponent fit (open circles). As mentioned above, at temperatures higher than 24°C the eighth exponent is redundant. Therefore, for further analysis at these temperatures we used the results from the seven-exponent fit. These exponents are labeled 1–8 in ascending order of half-times. At 20°C these components have half-times of about 1 μs, 6 μs, 30 μs, 100 μs, 500 μs, 1.5 ms, 5 ms, and 20 ms, respectively.

A linear dependence of apparent rate constants in the Arrhenius plots can only be expected in a case of sequential irreversible transitions when the apparent rate constants coincide with intrinsic ones. On the other hand, the curvature of an Arrhenius plot would indicate a more complex character of the relaxation scheme. However, when even the linear approximation is used, the accuracy of the apparent activation enthalpy and entropy values is often overestimated in the literature. The use of the standard least-squares linear fit in Arrhenius coordinates assumes a statistically significant number of experimental points and a random distribution of errors. The nonorthogonality of exponents in complex kinetics gives, in the case of relatively close apparent rate constants, very low reliability of statistical independence of errors. Furthermore, the temperature range of measurements is usually narrow (in our measurements it is 0–40°C or about 10% of absolute temperature), and the number of temperature points over this range is usually restricted by the complexity of the measurements.

As illustrated in Fig. 4, the derived set of eight exponents could be described almost equally well if we fixed one of the Arrhenius parameters and varied the other. The solid lines correspond to the simultaneous linear fit of apparent activation enthalpy and entropy of transitions (see Table 2). For τ_4 they are $\Delta E^{\#} = 52 \pm 3$ kJ/mol and $\Delta S^{\#} = 5 \pm 9$ J/mol K (errors were calculated assuming their randomness). If we fixed $\Delta S^{\#} = 0$ J/mol K for all rate constants, the apparent enthalpy barrier varied from 35 kJ/mol (τ_1) to 65 kJ/mol (τ_8) (dashed lines). If we fixed $\Delta E^{\#} = 50$ kJ/mol, the variation of $\Delta S^{\#}$ from +40 J/mol K (τ_1) to −40 J/mol K (τ_8) also approximated the Arrhenius behavior (dotted lines). This example provided the range of uncertainty in estimating the thermodynamic parameters, which yielded the vari-

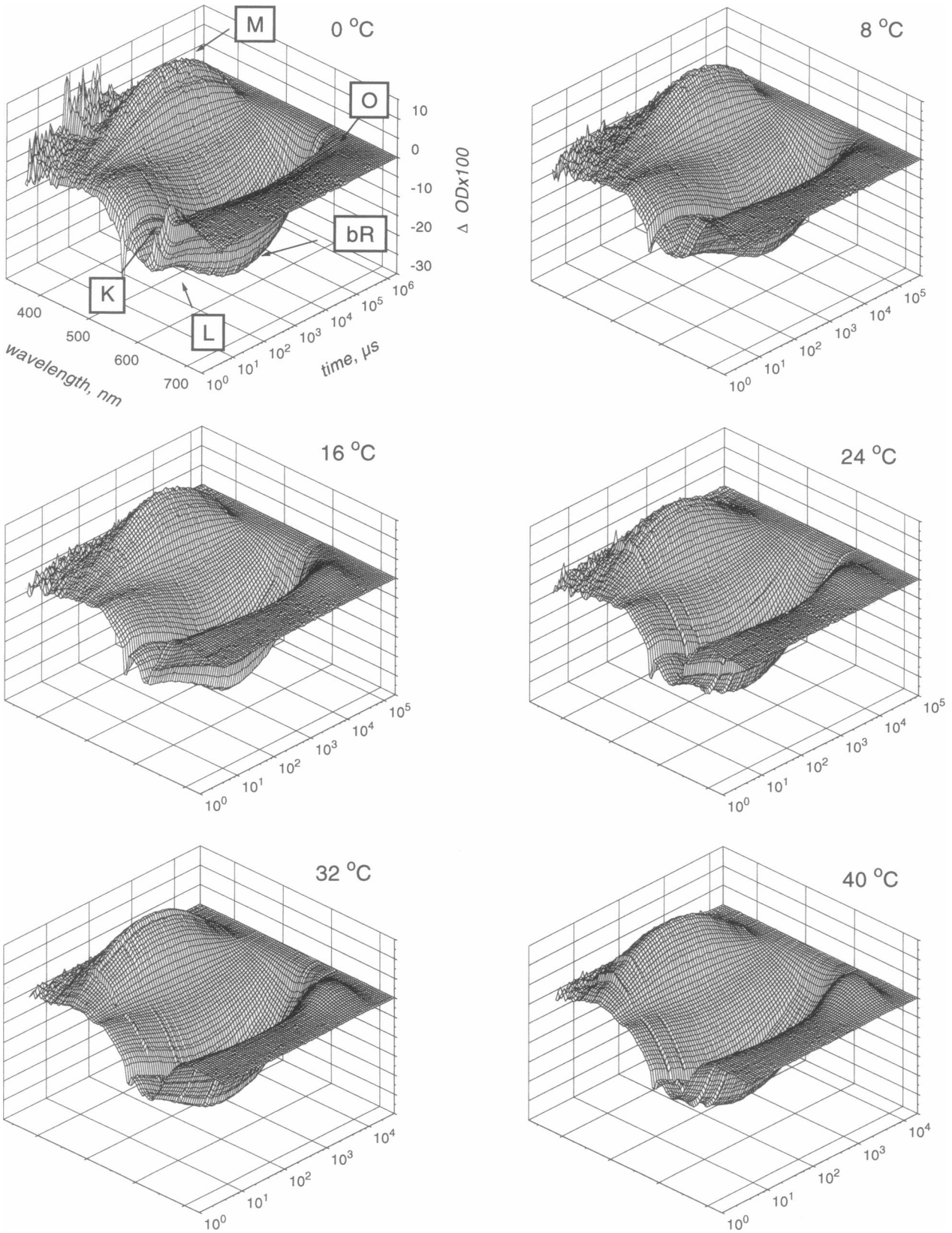

FIGURE 1 Experimentally measured differential transient spectra of the bR photocycle at different temperatures. Data at 4°C, 12°C, 20°C, 28°C, and 36°C are not drawn. Each temporal trace contains 100 points, which were obtained after quasilogariphmic data compression of the initial 6000 linear time points measured in three linear time windows (for the MEXFIT computing we used from 6000 to 400 data compression) measured from 330 to 730 nm with a resolution of 4 nm (101 spectral points).

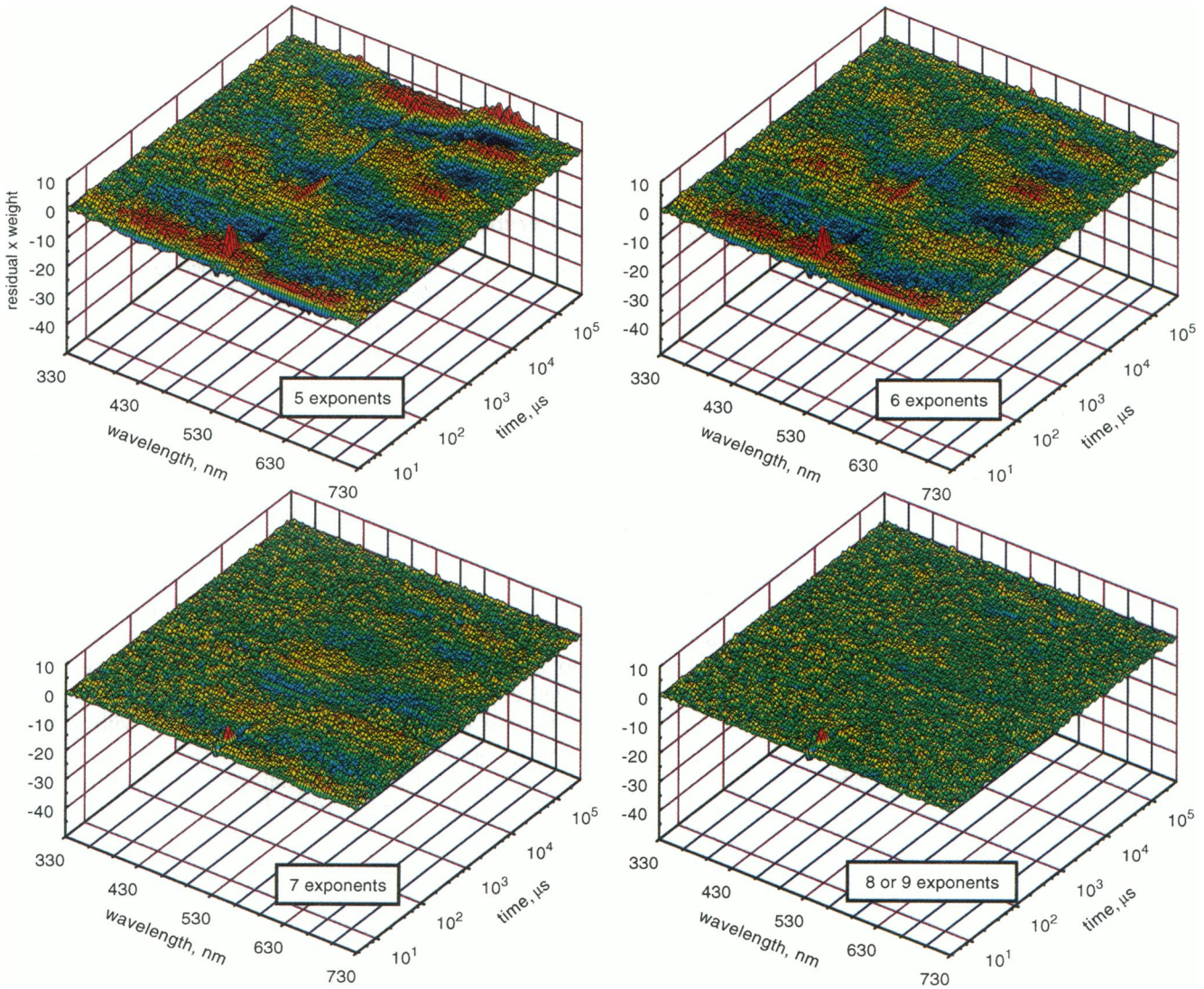

FIGURE 2 Three-dimensional surfaces of weighted residuals of five to nine exponential approximation of the bR transient absorbency changes at 8°C.

ation of measured half-times from 1 μs to about 20 ms (at 20°C) and very similar temperature dependencies in the relatively narrow temperature range. In this regard the estimated apparent activation parameters of τ_1 and τ_4 of Zubov et al. (1982) seem to be more reliable. Their data had much higher errors but were measured over a wider temperature range with more data points and therefore considerably improve the level of confidence.

In Fig. 5 we compare our eight apparent rate constants with two rate constants obtained by Zubov et al. (1982). In low-temperature experiments they used a water-glycerol suspension of bR, which slowed the main apparent component of the K decay (τ_1) but did not alter the main apparent component of the M rise (τ_4). (Zubov et al. (1982) have measured rate constants with single exponential approximation of absorption chages at 624 and 424 nm, where the K decay and M rise contribute significantly.) Unfortunately, only these two components of the photocycle kinetics after

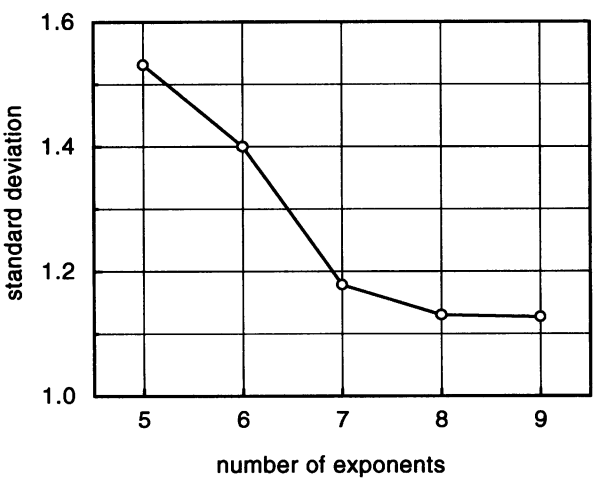

FIGURE 3 Dependence of standard deviation (SD) of weighted residuals on the number of applied exponents at 8°C.

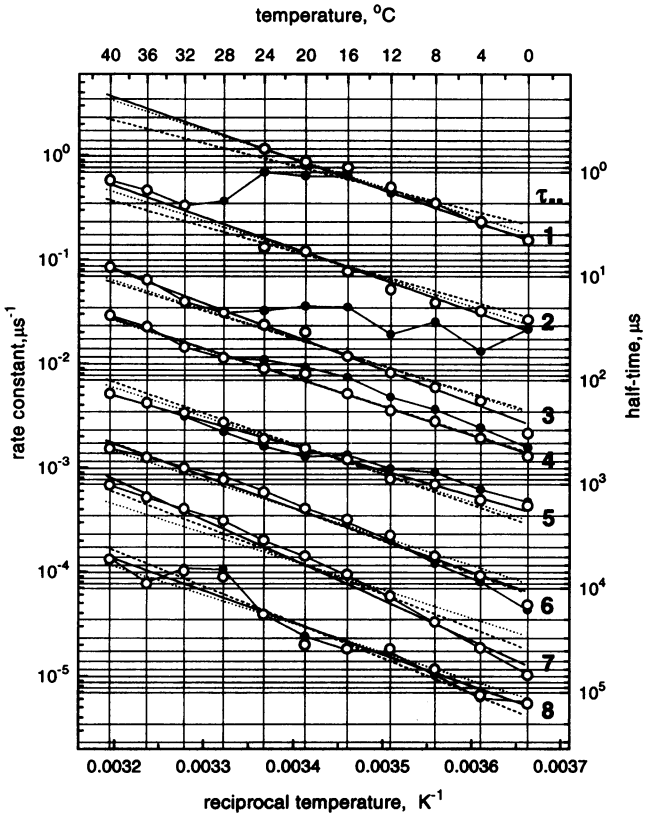

FIGURE 4 Arrhenius plots of the exponential component derived from experiments: seven (●) and eight (○) exponents of the data fit and apparent linear fit of activation parameters of eight components of the photocycle. ——, Both enthalpy and entropy of apparent activation were fitted simultaneously; – – –, fits of only enthalpies when entropy is fixed to zero for all components; ·····, fits of only entropies when enthalpy is fixed to 50 kJ/mol for all components (see discussion in the text).

the K intermediate have been measured over a wide temperature range. According to their results τ_1 and τ_4 could be measured down to −60 and −100°C, respectively, and show more or less straight dependencies in the Arrhenius coordinates. Although this is not a direct evidence of the irreversibility of this transition (and the absence of preceding reversible steps), it might be considered as an indication. For instance, in Fig. 5 τ_6 and τ_7 have well-pronounced curvatures that indicate a more complex relationship of apparent half-times and intrinsic transitions. The data in Fig. 5 also show the temperature range within which the photocycle kinetics must be measured to achieve more reliable results on both the components of relaxation and their temperature dependencies. From the data it can be explained why at temperatures below about −50°C an M decay has never been observed. With a model of the temperature-dependent quasiequilibrium (see discussion below), the simple extrapolation (τ_6 and τ_7) gives at this temperature a half-time of about 30 s and 10^3 s, respectively. The latter value represents the main component of decay of M and might be considered as an absence of transition. In Table 1 the half-times of eight exponents at different temperatures and in Table 2 the apparent activation parameters (for τ_6 and τ_7 we include the nonlinear estimation of intrinsic transitions in additional rows) are summarized. In Fig. 6 the present data are also compared with data of Xie et al. (1987) and Váró and Lanyi (1991b).

Differential spectra of exponents

Fig. 7 represents eight differential spectra of exponential amplitudes of the correspondent apparent half-times at different temperatures. Positive bands correspond to the decay of the transient absorption and negative bands correspond to the rise. As mentioned above, only eight exponents give smooth spectra and their dependencies upon the temperature. The most pronounced dependencies are indicated in Fig. 7 by arrows to show the directions of evolution of spectra with the growth of temperature. In two upper panels (τ_1 and τ_2) the sharp negative peaks are due to the scattered laser light at 530 nm. As indicated above, the fastest component (τ_1) in our experiments could be resolved only at temperatures below 24°C. Therefore currently we are not confident that growth of a positive band in the panel of τ_1 is not a computational artefact, because these amplitudes were fitted at high temperatures from the tail of the exponent. This must be clarified in new experiments with a higher time resolution.

Comparison of the differential spectra of τ_8 (Fig. 7) with data of Hofrichter et al. (1989) (figure 4c of their paper) at 25°C, as well as the similarity of derived rate constants (~40 s^{-1} of our data and their k_{III} = 29 s^{-1} of the 13-*cis* cycle), led us to the conclusion that this component in our data comes from a small contribution of the 13-*cis* cycle to the measured kinetics. Using the relative spectral amplitude of this component in the dark-adapted cycle in Fig. 4 of Hofrichter et al. (1989), we estimate this contribution to be about 5–10% of all cycling molecules. Moreover, when we used this component in the evaluation of spectra of intermediates (see Discussion), the contribution of this component to the spectra of the P_5 (a state that forms with a half-time of 100 μs) does not permit us to obtain the absolute spectra of the M intermediate without significant distortion of the baseline in the red region of the spectra. However, we cannot exclude the possibility that, especially at low temperatures, this component arises at least partially from the all-*trans* cycle because it contains some differential absorption in the blue region, where according to Hofrichter et al. (1989) no significant changes have been found in the 13-*cis* cycle (however, they did not investigate the temperature dependence). The relative contribution of τ_8 is small. Therefore, we exclude this component from the following analysis, although it gives a systematic error of about 5–10% in the estimation of the overall cycling fraction and a distortion of the spectra of K and L intermediates in the blue. However, this distortion is insignificant compared to other sources of error that determine the spectral resolution.

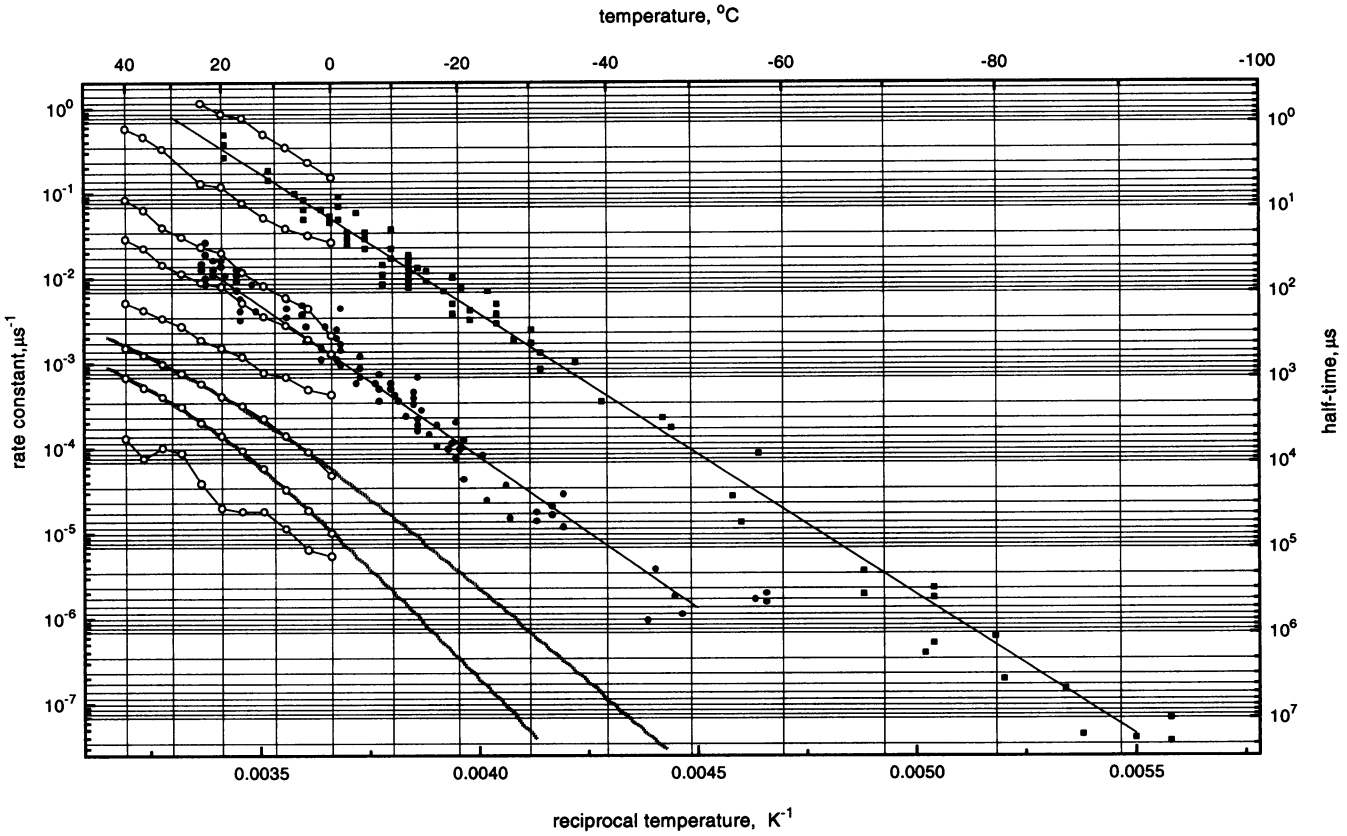

FIGURE 5 Comparison of the eight half-times (○) with data of Zubov et al. (1982) (● and ■). Two solid gray lines are the nonlinear fit of τ_6 and τ_7 (see discussion in the text).

TABLE 1 Apparent half-times of the bR photocycle at different temperatures

T (°C)	τ_1 (μs)	τ_2 (μs)	τ_3 (μs)	τ_4 (μs)	τ_5 (μs)	τ_6 (μs)	τ_7 (μs)	τ_8 (μs)
0	4.6	35.2	325	762	2310	13,860	69,300	128,800
4	3.1	21.6	154	361	1386	7700	34,700	108,000
8	2.0	16.5	111	249	1083	4620	23,100	69,300
12	1.4	12.0	82	196	937	3010	11,550	34,650
16	1.0	8.3	57	134	630	2100	7700	34,650
20	0.8	5.9	35	91	478	1690	4950	23,100
24	0.6	5.2	28	77	377	1170	3460	17,300
28	0.5	3.6	23	61	309	825	2240	5780
32	—	2.7	18	49	209	690	1730	6300
36	—	2.4	12	33	164	550	1330	11,500
40	—	2.3	9.5	26	135	456	1020	5800

The spectra of τ_1 (Fig. 7) show a single isosbestic point and, as is generally accepted, correspond to the difference spectra between K and L intermediates, and a contribution of the following states in the reaction cycle is small as a ratio of half-times of the formation and decay of L. If the K decays irreversibly, the summation of amplitude spectra of all following derived components would give the differential spectra of the K-bR with a contribution of the nearest later state (L) less than $\sim \times 10^{-5}$. Within this accuracy one can treat all of the following steps with the following initial conditions: at $t = 0$ the probability of finding the molecule in the state is $K = P_1 = F_c$, and the probabilities of finding all of the intermediates are $P_2 \cdots n = 0$, where the cycling fraction is $F_c = N_c/N_o$ (with N_c of total N_o bR molecules undergoing the cycle upon the excitation pulse) and n is the number of intermediates (exponents) found on the relaxation pathway. Below we apply this assumption to the kinetic scheme of relaxation.

DISCUSSION

In the following discussion the data set is used to derive a sequential irreversible model of the bacteriorhodopsin pho-

TABLE 2 Apparent activation parameters of the bR photocycle

	τ_1	τ_2	τ_3	τ_4	τ_5	τ_6	τ_7	τ_8
$\Delta E^{\#}$ (kJ/mol)	50 ± 3	47 ± 2	55 ± 3	52 ± 3	47 ± 2	57 ± 3 36 ± 25	72 ± 3 37 ± 26	56 ± 6
$\Delta S^{\#}$ (J/mol K)	40 ± 10	11 ± 7	23 ± 9	5 ± 9	−25 ± 5	−1 ± 9 −67 ± 75	42 ± 9 −70 ± 80	−25 ± 20

For explanation see text. Errors are given as standard, therefore we assume random distribution of data points around linear dependence in Arrhenius coordinates. The nonlinear estimation of intrinsic barriers is given for τ_6 and τ_7 as second values. See discussion in the text.

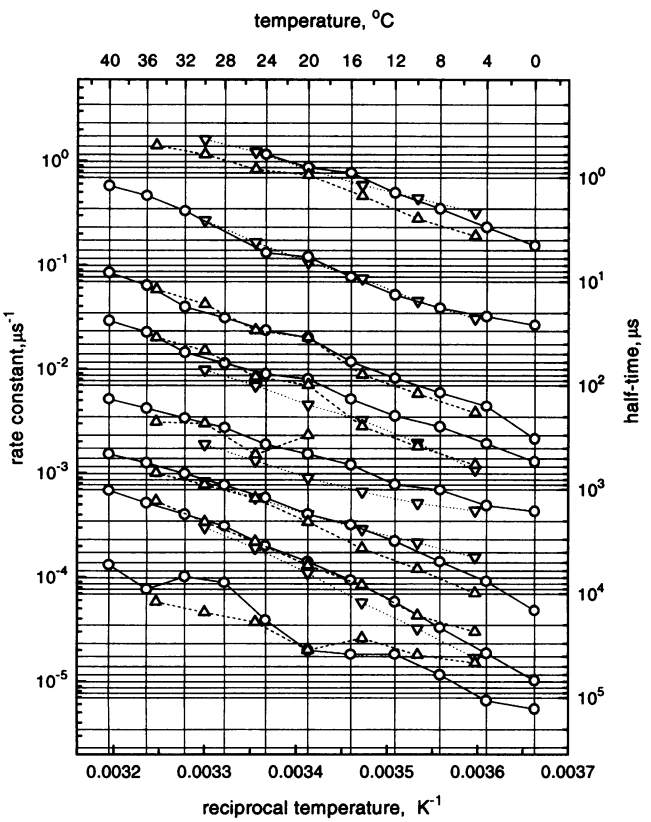

FIGURE 6 Comparison of the eight half-times (○) with seven exponents derived by Xie et al. (1987) (△) and six apparent exponents of Váró and Lanyi (1991b) (▽).

tocycle. It should be stressed that this model is one plausible scheme for explaining the data. However, it has certain advantages over other published schemes: 1) it is relatively simple and contains only a single free parameter, namely the cycling fraction; 2) it explains the data over the wavelength-to-temperature range; and 3) it should be possible, in principle, to test the spectrally silent transitions found in this work by other spectroscopic methods, e.g., Fourier transform infrared spectroscopy. Before the model is introduced and discussed, the experimental data are compared with those from the literature to establish a common data base that is generally accepted, thus avoiding discussion about the validity of the original data.

Comparison of the derived kinetic coefficients with literature data

To compare our results with those given in the literature we combine in Fig. 6 our half-times with the seven derived at pH 7 by Xie et al. (1987) (Fig. 6, Δ) and with the six of Váró and Lanyi (1991b) (Fig. 6, ▽). Whereas the data of Xie et al. (1987) were directly taken from figure 6b of their paper, the intrinsic rate constants of Váró and Lanyi (1991b, Fig. 5 of their paper) were converted to the apparent ones by using the model K ↔ L ↔ M1 → M2 ↔ N ↔ O→ bR plus N → bR proposed by the authors. It is apparent that the data measured earlier coincide quite well with those presented here.

Although in the work of Xie et al. (1987) τ_2 (6 µs) was not resolved, the other seven exponents generally come close to those in our experiments. Because in their analysis τ_2 is missing and τ_5 is unresolved at low temperatures, the values of τ_1, τ_3, τ_4, and τ_6 (in the range 5–20°C) are greater (see Fig. 6). These deviations are not significant. Therefore, it can be concluded that the data base described by Xie et al. (1987) and the present data with the exception of the eighth exponent (τ_2 in Fig. 4) are congruent.

A similar correspondence is also found with the data of Váró and Lanyi (1991b), if their published intrinsic rate constants are converted into the apparent rate constants (Fig. 6). Their fit of the K-to-L transition gave an almost irreversible reaction; therefore, k_{KL} coincides with the fastest resolved half-time (τ_1). The three intrinsic transitions, L ↔ M1 → M2, gave two apparent half-times: τ_2, which in their model corresponds to L ↔ M1, and τ_4, which corresponds to the M1→M2 irreversible step of their model. It is interesting to see that according to the model of Váró and Lanyi (1991b), the deprotonation of the SB (L ↔ M1) has to occur much faster (τ_2 = 6 µs at 20°C) than the main component of the absorption rise in the blue (τ_4 = 100 µs), which is M1 → M2 of their model. Finally, the last part of the photocycle scheme of Váró and Lanyi (1991b), M2 ↔ N ↔ O → bR plus N → bR, gave three apparent half-times that are close to our τ_5 (their N ↔ O quasiequilibrium), τ_6, and τ_7 (decay of M, growth and decay of N + O). The data of Váró and Lanyi (1991b) do not provide information on τ_3 and τ_8.

In a third comparison the data are analyzed together with results published by Zubov et al. (1982), who determined the rate constants over a large temperature range. As can be

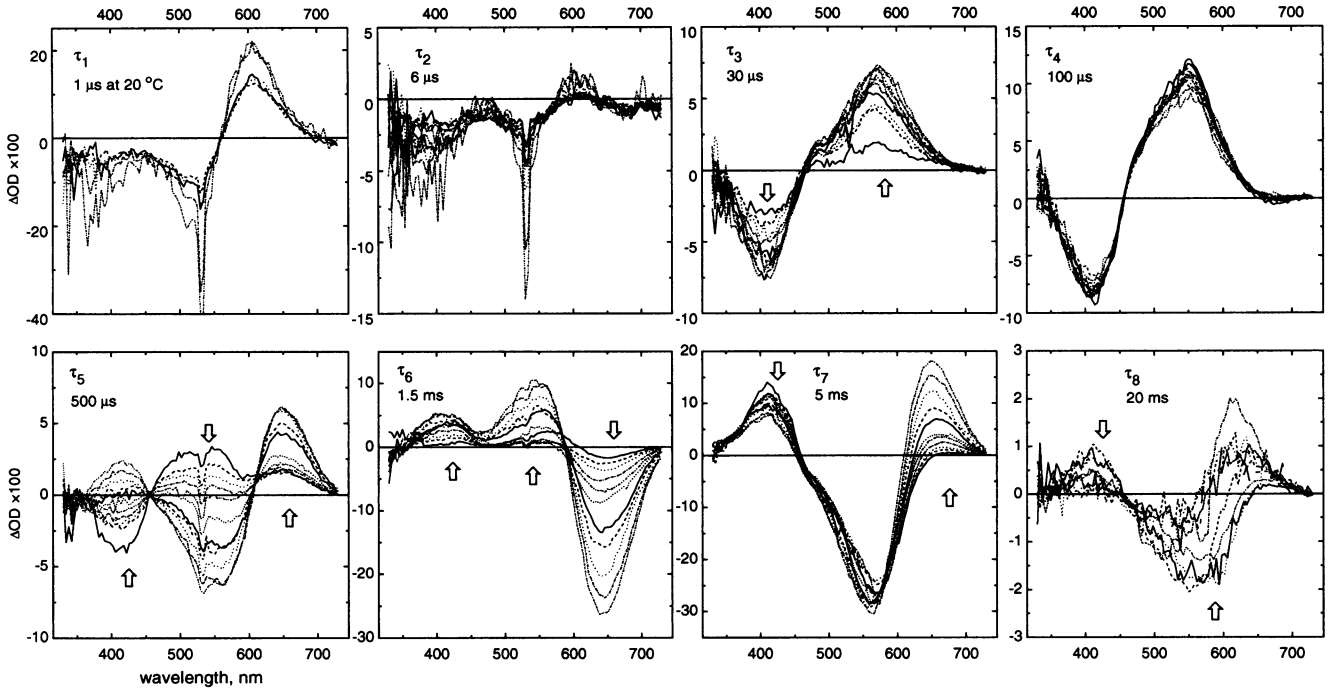

FIGURE 7 Differential spectra of amplitudes of eight exponents at different temperatures. For the fastest component (τ_1) the spectra at $T > 20$°C are excluded as not well resolved. In each panel arrows indicate directions of spectra evaluations with growth of temperature.

seen from Fig. 5, the reactions corresponding to τ_1 and τ_4 are quite similar to our data showing a linear Arrhenius behavior.

All four of these data sets are within the same limits of error. This is quite important because it states that despite different models published in the literature, the original data seem to be comparable and not to be dependent on the laboratory or the particular sample. Therefore, it should be possible to find a common answer to the bacteriorhodopsin photocycle.

Linear irreversible model of the photocycle

So far, the major problem of designing a reasonable model of the photocycle has been that the number of exponentials is greater than the spectroscopically unequivocally identified number of intermediates. In the present work seven exponentials are necessary to describe the all-*trans* photocycle, indicating that a model of the photocycle must comprise at least seven intermediates. To elucidate possible mechanisms the original linear scheme of conversions with irreversible transitions was analyzed first.

For the given set of exponents (half-times and their amplitude spectra), there is only a single case for which the problem of deriving the spectra of intermediates has an exact solution—this is the sequence of irreversible transitions between intermediates. Even this case would give by permutation $n!$ submodels with different assignments of apparent half-times to the intrinsic transitions. Many of them might be unrealistic and can therefore be withdrawn from further analysis. As discussed in the Results, we found that the slowest component (τ_8) is a contribution to the kinetics of the 13-*cis* photocycle. Therefore, in the following analysis this component is omitted.

With the exception of two permutations, all other permutations of half-times gave unrealistic spectra, i.e., the absolute spectra of the derived states had much higher absorbencies than the ground state or negative bands. Reasonable results were obtained with two models A and B of an irreversible sequence of transitions. Model A has an ascending order of half-times, i.e., $\tau_1 < \tau_2 < \tau_3 < \tau_4 < \tau_5 < \tau_6 < \tau_7$ are the half-times of the corresponding reactions and coincide with an assignment of experimental values.

$$P_1 \overset{\tau_1}{\rightarrow} P_2 \overset{\tau_2}{\rightarrow} \cdots P_6 \overset{\tau_6}{\rightarrow} P_7 \overset{\tau_7}{\rightarrow} bR. \qquad \text{(A)}$$

The general analytical solution of this irreversible sequential scheme of a first-order relaxation is given in the Appendix. When this procedure was applied to the spectra of exponentials (Fig. 7), the differential spectra of intermediates $P_1 \cdots P_7$ have been calculated using Eq. 6 of the Appendix (Fig. 8). A common term, $1/F_c$, of Eq. 6 was omitted from this calculation, but when the differential spectra were converted to absolute, this single unknown value of the model was determined by using criteria discussed in the next section. In the second model (B) τ_6 and τ_7 are exchanged, resulting in the following scheme:

$$P_1 \overset{\tau_1}{\rightarrow} P_2 \overset{\tau_2}{\rightarrow} \cdots P_7 \overset{\tau_7}{\rightarrow} P_6 \overset{\tau_6}{\rightarrow} bR. \qquad \text{(B)}$$

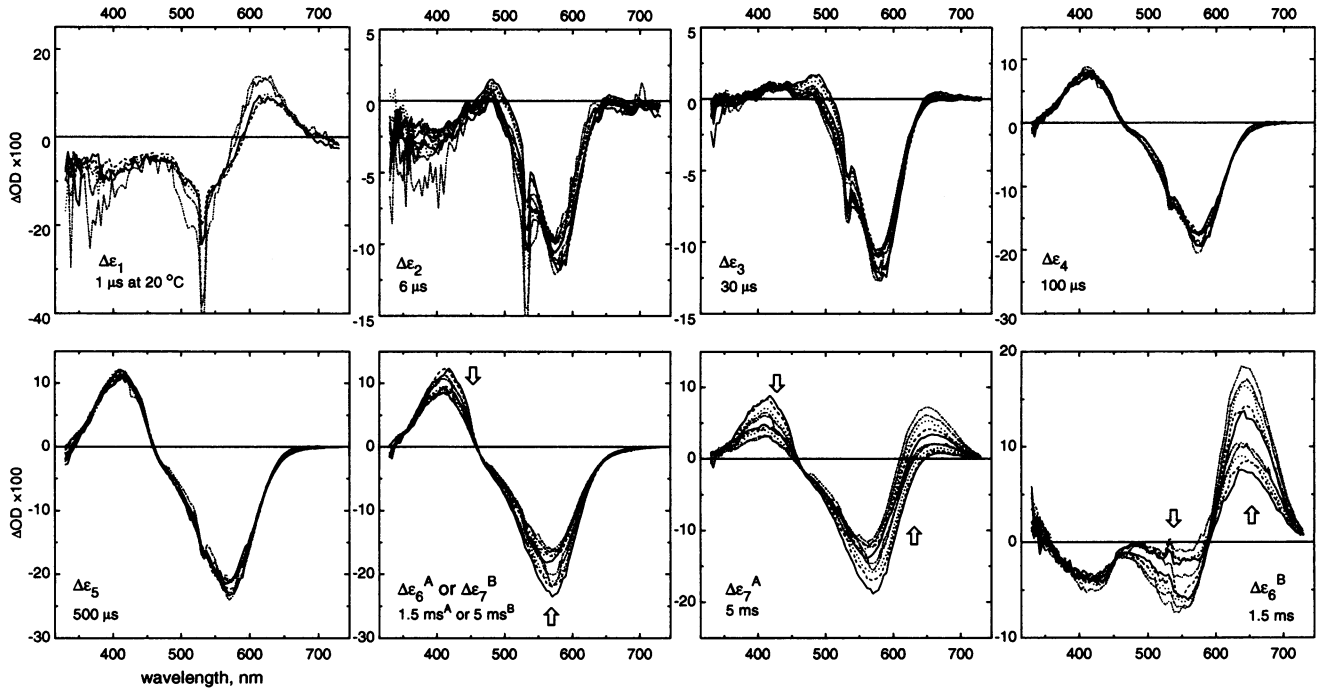

FIGURE 8 Renormalized differential spectra of seven intermediates of the all-*trans* bR photocycle derived from the sequential irreversible scheme of relaxation (submodels A and B) at different temperatures.

As will be discussed below, submodel B is more congruent with the literature data than submodel A.

An analogous approach has been used by Milder et al. (1991) and Hofrichter et al. (1989) to derive the spectra of intermediates. Although the first group did not find in their data analysis the exponential components that we assigned here as τ_2, τ_5, and τ_8, and the second group missed τ_2 and τ_5 (the probable reasons will be discussed below), there are many coincidences between the spectra $\Delta\epsilon_1$, $\Delta\epsilon_3$, $\Delta\epsilon_4$, $\Delta\epsilon_6^A$, and $\Delta\epsilon_7^A$ (Fig. 8) and the spectra designated as I-V in figure 2b of Milder et al. (1991) and in figure 4a of Hofrichter et al. (1989).

Spectra of intermediates

To obtain the absolute spectra of P_i states of an irreversible sequence, one has to find only the single unknown: the cycling fraction F_c (see the Appendix). We used differential spectra $\Delta\epsilon_5$ (Fig. 8) of state P_5 to obtain this value. As seen in Fig. 8, these spectra are temperature independent and have maximum absorbency changes and a simple two-lobe form. The spectra of the P_5 state at $F_c = 0.26 \pm 0.01$ are shown in Fig. 9 (ϵ_5 panel). All other spectra in Fig. 9 have been calculated using this fixed value. The error is estimated at each temperature as the possible variation of F_c that does not produce a variation of the baseline from 470 to 730 nm (ϵ_5 panel in Fig. 9) that exceeds the thickness of the light grey baseline, which was subsequently fitted as a second-order polynomial (see Table 3). The variation of F_c between different temperature measurements was 0.04 (or about 10%), but because the shape of spectra $\Delta\epsilon_5$ (Fig. 8) was essentially temperature independent, we eliminate this higher variance by renormalization of $\Delta\epsilon_5$; all spectra in Fig. 8 are also renormalized by using the values obtained at different temperatures upon renormalization of $\Delta\epsilon_5$. Because some spectra contain systematic errors from the non-random variation of the excitation level, we depicted in Fig. 9 the absolute spectra at two temperature points, 8°C and 40°C, where no significant systematic errors were found in the spectra.

The temperature changes observed only for ϵ_6 and ϵ_7 (for both submodels) between these limits might be reliably interpolated from the temperature behavior of the differential spectra (Fig. 8) as well as extrapolated to 0°C. The only exception is spectra ϵ_1, where the fastest component was not resolved at 40°C. At 8°C this component has a very noisy spectrum in the blue range; therefore these points are omitted, but its main feature (e.g., it is lower than the β-band of ground bR absorbency) is reliable (compare with $\Delta\epsilon_1$ in Fig. 8) and coincides with literature data. The half-times of each state referred to 20°C (see Table 1) are also depicted in Fig. 9. In a recent article Nagle et al. (1995) tested the bR photocycle using essentially the same procedure (variation of the cycling fraction) to derive the spectra of intermediates of the bR mutant D96N. Their temperature-independent (5–25°C) spectra of M (Fig. 3) coincide well with our result.

The spectrum of bR_{570} and the spectra of all intermediates depicted in Fig. 9 have been fitted as skewed Gaussian curves (Metzler and Harris, 1978; Birge, 1990). In Fig. 9 the light gray lines are the best fit of the ground bR_{570} (ϵ_0)

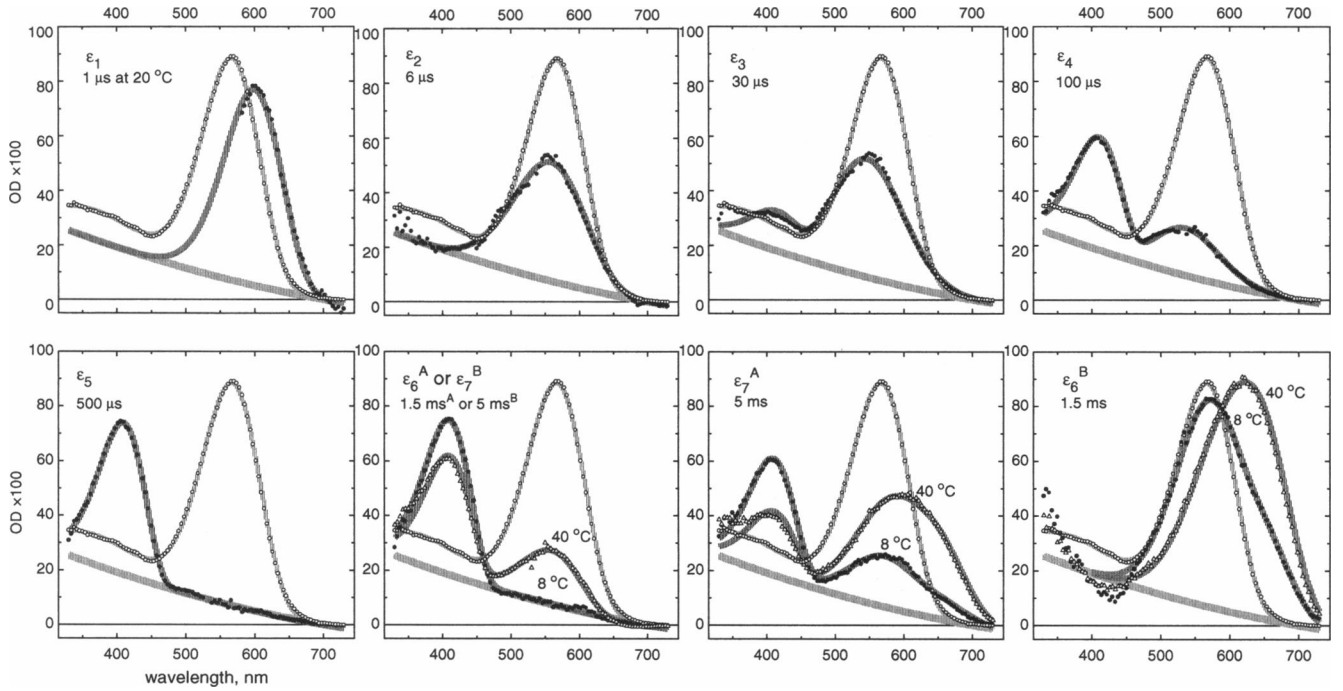

FIGURE 9 Absolute spectra of intermediates and their quasiequilibrated mixtures, which decay with seven distinct rate constants in the all-trans bR photocycle. At first, the ϵ_5 spectra (●, half-time 500 μs at 20°C) were derived from corresponding $\Delta\epsilon_5$ (Fig. 8) differential spectra, using variation of the cycling fraction F_c to achieve singular bandshape. Within the thickness of gray solid line (single Gaussian plus second-order polynomial as background scattering) these spectra are temperature independent. These parameters of the $\Delta\epsilon_5$ nonlinear spectral fit have been used then in the fitting of other spectral intermediates in Fig. 9 (● and △ and correspondent grey solid lines as their best fitting). In each panel open cycles and corresponding solid light grey lines represent the ground bR spectra and their fitting (see Table 3).

spectra, and the dark gray lines are the fits of the intermediate spectra with one, two, or three maxima. All parameters of the nonlinear least-squares fitting are given in Table 3. Initially the spectrum ϵ_5 was fitted as a single Gaussian band plus the baseline. By using these parameters of the baseline the ground bR_{570} spectrum was approximated by two Gaussian bands. The fine structure of the weaker β-band ($\lambda_{max} \approx$ 374, 397, and 424 nm) (Becher and Cassim, 1976) was not well resolved and therefore was approximated as a single band. Among the seven intermediates of our model there are only three states that have a single maximum: ϵ_1 (the K intermediate), ϵ_2 (the L intermediate), and ϵ_5 (the M intermediate). All others are mixtures of L and M (ϵ_3, ϵ_4), M and N (ϵ_6^A and ϵ_7^B), M and N and O (ϵ_7^A), and N and O (ϵ_6^B). We also found that spectra corresponding to ϵ_2, ϵ_3, ϵ_4, and ϵ_5 are essentially temperature independent, whereas ϵ_6 and ϵ_7 show significant changes in the relative proportion of the intermediates with temperature. The apparent shift of the maximum of ϵ_2, ϵ_3, and ϵ_4 bands from 559 to 537 nm (see Table 3) we attribute to the laser artifact. Indeed, the scattered laser light (532 nm) distorts the shape of spectra just around this wavelength as much as shorter half-times of the states (compare spectra $\Delta\epsilon_1$, $\Delta\epsilon_2$, $\Delta\epsilon_3$, $\Delta\epsilon_4$ in Fig. 8). Therefore, the last value ~540 nm is a most reliable determination of the maximum of the L state. This distortion gives much less systematic error in the determination of the relative partition of L and M in these spectra.

From the spectral fit of components we estimate the relative contribution of M and L as about 2:8 for ϵ_3, and 7:3 for ϵ_4, whereas the spectra ϵ_6^A (or ϵ_7^B) at the low temperature limit are almost 100% of M, and at 40°C is about 75% of M and 25% of N intermediates (assuming that the extinction of the N is close to that of bR_{570}). (The P_3 state probably contains some features of the β-band of the L-intermediate because the spectral fit with only two bands (L and M) gives sytematic deviation in the region 330–400 nm (see the spectra ϵ_3 in Fig. 9). Therefore the partition of M in this state might be slightly overestimated.) Between these limits the partition of N to the P_6 (or P_7 of submodel B) state increases gradually with an accompanying decrease in M. As noted earlier, submodels A and B in Figs. 8 and 9 correspond to ascending and descending orders of the assignment of the half-times to intrinsic ones, respectively. In submodel B the intermediate P_6 is the quasiequilibrium of only two spectral forms in the visible range (namely, N and O) and is therefore preferable over submodel A, where three maxima were found (M, N, and O) (see Fig. 9). At high and low temperature limits, this equilibrium is almost fully shifted to N or to O, respectively. These observations are in agreement with the results of Chernavskii et al. (1989),

TABLE 3 Parameters of the Gaussian fit of spectra of the bR photocycle in Fig. 9*

	χ^2	A_{1max} (OD × 100)	ρ_1	$\Delta\nu_1$ (cm^{-1})	λ_{1max} (nm)	A_{2max} (OD × 100)	ρ_2	$\Delta\nu_2$ (cm^{-1})	λ_{2max} (nm)	A_{3max} (OD × 100)	ρ_3	$\Delta\nu_3$ (cm^{-1})	λ_{3max} (nm)
ϵ_0	0.6	11 ± 0.3	1.6 ± 0.4	12,000 ± 2000	370 ± 3	81.5 ± 0.2	1.4 ± 0.02	3120 ± 34	568 ± 1				
ϵ_1	3.8									73 ± 1	1.4 ± 0.3	2800 ± 200	600 ± 5
ϵ_2	3.8	−0.4 ± 0.6	1.6	4920	410	43.6 ± 0.5	1.4 ± 0.04	4064 ± 63	559 ± 1.5				
ϵ_3	4.2	13.8 ± 0.6	1.6	4920	410	43.3 ± 0.6	1.2 ± 0.04	4062 ± 63	547 ± 15				
ϵ_4	1.1	41.1 ± 0.3	1.6	4920	410	17.4 ± 0.3	1.2 ± 0.05	3857 ± 82	537 ± 1.5				
ϵ_5	0.6	55.6 ± 0.2	1.6 ± 0.02	4920 ± 30	410 ± 1								
ϵ_6^A, ϵ_7^B (8°C)	1.5	56.6 ± 0.4	1.6	4920	410	0.5 ± 0.3	1.4	3340	561	−0.4 ± 0.3	1.4	3100	632
ϵ_6^A, ϵ_7^B (40°C)	4.5	43.3 ± 0.6	1.6	4920	410	20.3 ± 0.5	1.4	3340	561	−1.4 ± 0.5	1.4	3100	632
ϵ_7^A (8°C)	1.7	42.5 ± 0.3	1.6	4920	410	14.2 ± 0.4	1.4	3340	561	8.8 ± 0.3	1.4	3100	632
ϵ_7^A (40°C)	7.5	23.0 ± 0.7	1.6	4920	410	20.7 ± 0.8	1.4	3340	561	34.4 ± 0.7	1.4	3100	632
ϵ_6^B (8°C)	1.6					57.9 ± 0.4	1.4 ± 0.03	3340 ± 30	561 ± 1.5	37 ± 0.7	1.4	3100	632
ϵ_6^B (40°C)	0.7					18.2 ± 6	1.4	3340	561	81 ± 1	1.4 ± 0.06	3100 ± 200	632 ± 5

*The skewed Gaussian function (Metzler and Harris, 1978; Birge, 1990):

$$A(\nu) = A_{max} \times \exp\left\{-\frac{\ln 2}{(\ln \rho)^2}\left[\ln\left(\frac{(1/\lambda - 1/\lambda_{max})(\rho^2 - 1)}{\Delta\nu\rho} + 1\right)\right]^2\right\}, \quad \nu > \nu_{max} - \frac{\Delta\nu\rho}{(\rho^2 - 1)}; \quad A(\nu) = 0, \quad \nu \le \nu_{max} - \frac{\Delta\nu\rho}{(\rho^2 - 1)}$$

has been used to fit spectral bands. ϵ_0 is the bR ground spectra depicted in all panels of Fig. 9 for comparison. The background scattering lines (thick gray line in all panels of fig. 9) have been fitted as $A + B\lambda + C\lambda^2$ from ϵ_5 spectra ($A = 63 \pm 4.5$, $B = -0.14 \pm 0.02$, $C = (7 \pm 1)10^{-5}$, λ in nm). Values without standard errors written under them mean that they were fixed in given nonlinear fit.

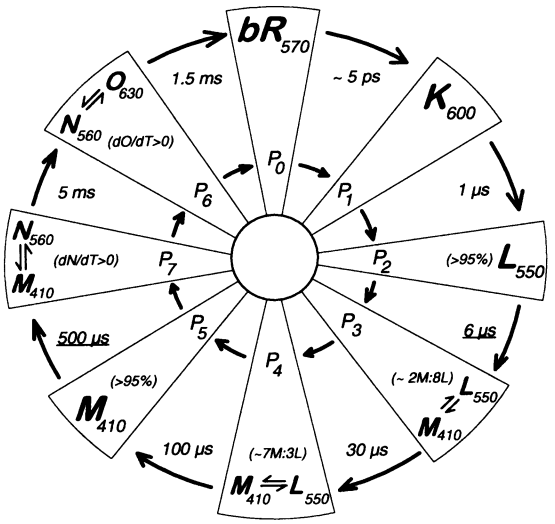

FIGURE 10 The scheme of the bR photocycle based on the sequential irreversible model of relaxation (submodel B) and the interpretation of derived complex spectra of correspondent intermediates in Fig. 9. Two underlined half-times indicate the possible assignment of transitions to the quasiequilibration (see Discussion).

whose temperature pulse experiments showed that the fast temperature-induced growth of the O intermediate occurred from N but not from the M intermediate. The ratio N:O in submodel B is estimated as 75:25 at 8°C and as 25:75 at 40°C (again assuming that $OD_{Nmax} \approx 0.8$). Using the law of conservation of matter, this gives the $OD_{Omax} \approx 1$. It is interesting to note that according to submodel B, the path of reprotonation of the Schiff base $P_7 \rightarrow P_6 \rightarrow bR$ has a descending order of half-times, in contrast to the deprotonation path $P_2 \rightarrow P_3 \rightarrow P_4 \rightarrow P_5$, in which the half-times become slower. A similar feature has been shown by Imamoto et al. (1992) in the photocycle of the phoborhodopsin from *Natronobacterium pharaonis*.

Kinetic model of the bR photocycle

The question now arises, do these spectra (Fig. 9) belong to distinct intermediates, or do they reflect the inappropriateness of the applied kinetic scheme? We would like to propose a novel scheme of the bacteriorhodopsin photocycle that assumes fast equilibration of some intermediates. Such a process cannot be kinetically resolved if the previous transition is slower but would result in a spectrum of a mixture of distinct spectral intermediates. Therefore the proposed model contains some transitions corresponding to the change of quasieqilibrium constant rather than new spectral intermediates, i.e., they are spectrally silent in the visible absorption range. This hypothesis is based on the reasonable assumption that some functionally significant transitions of the protein (e.g., protonation-deprotonation of the peripheral to the chromophore groups, conformational transitions) may not affect the visible spectra of chromophore. Moreover, it is easy to show that such a transition would contribute to the visible kinetics even if the visible spectra of states do not change at all (see Appendix).

Such a kinetic scheme of the bR photocycle based on submodel B is shown in Fig. 10. The four states P_3, P_4, P_7, and P_6 are quasiequilibria of the spectrally distinct states of bR (L, M, N, and O), implying that the rate of their equilibration must be faster than the fastest rate constant of the formation or decay of such a complex. Within our spectral resolution the analysis has shown that a factor of 5 as a lower limit would be sufficient.

Generally, this model does not permit the assignment of irreversible transitions to or from quasiequilibria to a particular state of such a pair (or to both of them). Nevertheless, a further simplification of the scheme in Fig. 10 can be made. The state P_2 ($L_{540} > 95\%$) decays with the half-time τ_2 (6 μs) to a quasiequilibrium between the same spectral intermediate L_{540} and M_{410}. The following slower process (30 μs) changes the quasiequilibrium constant from ~0.25 (2:8) to 2.3 (7:3). Therefore, we can assign the half-time τ_2 as the kinetic coefficient of equilibration of L_{540} and M_{410}, thus making this parameter not an irreversible transition but a result of the forward and back reactions of the quasiequilibrium. The same procedure (with even higher reliability: 5 ms/500 μs = 10) may be applied to the transition $P_5 \rightarrow P_6$, so that the half-time τ_5 (500 μs) may be assigned to the $M_{410} \leftrightarrow N_{560}$ equilibration. These two possible reassignments of the apparent half-times τ_2 and τ_5 are underlined in Fig. 10. The transitions $P_3 \rightarrow P_4$, $P_4 \rightarrow P_5$ and $P_7 \rightarrow P_6$ are spectrally silent, i.e., they do not produce new spectral forms in the visible region. Below we show how an assignment of the irreversible transitions τ_7 (5 ms) and τ_6 (1.5 ms) to the particular states of quasiequilibria in Fig. 10 has been made.

The irreversible transition with the half-time τ_4 (100 μs) might be considered as a "molecular switch," as proposed earlier (e.g., Váró and Lanyi, 1991a; Oesterhelt et al., 1992), which changes access of the Schiff base from the extracellular side to the cytoplasmic side. It is interesting to note that this constant is close to the apparent half-time (~150 μs; see Fig. 6) that was assigned in the model of Váró and Lanyi (1991b) to an irreversible M1 → M2 transition. Before this step the bR molecule undergoes a multistep decrease in the degree of protonation of the Schiff base from P_2 (100% of L) to P_5 (100% of M). In each step this degree (or the L/M ratio) is essentially temperature independent (see Fig. 9). This means that the fast reversible quasiequilibrium (L ↔ M) does not contain significant enthalpy and entropy changes between L and M. Indeed, within the accuracy of derived spectra in Fig. 9, the variance of spectra ϵ_2 to ϵ_5 with temperature does not exceed about 10%. Therefore, it is easy to show that the upper limit of enthalpy changes estimated from the temperature-insensitive L/M ratio does not exceed $\Delta E_{ML} = E_M - E_L \leq 2\text{–}3RT = 5\text{–}7$ kJ/mol, and depending on the absolute values of this ratio, the entropy changes vary from between 3 to 5 times R, giving 25–40 J/mol K (L/M → ∞) to less than R = 8.3 J/mol K (L/M → 0). Assuming that the L → M step corresponds

to a jump of the Schiff base proton to the nearest acceptor, the estimated values suggest a small difference in energy (enthalpy) and the degrees of freedom (entropy) between these two states. It appears that there are two steps in the conformational (or another spectrally silent) relaxation (30 and 100 μs at 20°C), which have been found in this analysis to be the slight modification of the relative free energy of the proton on the Schiff base and the primary acceptor group (-s) (mainly through the small entropy change) and forcing the proton to leave the Schiff base.

The situation drastically changes for the path of reprotonation of the Schiff base. The M ↔ N equilibrium that arises after P_5 (100% of M) has significant temperature dependence (see the ϵ_6 spectra in Fig. 9) as well as the N ↔ O (the ϵ_{7b} spectra). These dependencies provide a good explanation of the pronounced curvatures of the half-times τ_6 (1.5 ms at 20°C) and τ_7 (5 ms) in the Arrhenius plot (see Fig. 5), which correspond to the decay of the N ↔ O and M ↔ N quasiequilibrium, respectively, according to the submodel B. Indeed, these curvatures of the Arrhenius plot mean that the observed half-times depend on the temperature not only through the enthalpy barrier of thermal activation of this transition but also on the quasiequilibrium constant of M ↔ N and N ↔ O. This indicates that these rate-limiting transitions are induced by only one of the states (e.g., N or O but not both); otherwise the half-time would be insensitive to the changes in this quasiequilibrium. Therefore, both submodels N ↔ O → bR and O ↔ N → bR can explain the curvature of τ_6 as the effect of multiplication of intrinsic rate constant k_{ObR} or k_{NbR} on the temperature-dependent equilibrium constants O/(O + N) or N/(O + N), correspondingly. Because O/(O + N) approaches unity with an increase in temperature, the rate constant k_6 (= ln $2/\tau_6$) goes to k_{ObR} asymptotically at the high temperature limit in the case N ↔ O → bR, and k_6 goes to k_{NbR} at the low temperature limit in the case O ↔ N → bR. It is interesting to note that this case can principally give the bell-like Arrhenius behavior (e.g., after acceleration of the apparent rate constant, up to the temperature beyond which a further increase in temperature might result in a deceleration of the rate constant). We found that in the first case the estimated barriers of enthalpy and entropy of activation are very close to the parameters of the preceding apparent transitions (τ_1 to τ_5), whereas the submodel O ↔ N → bR gives the about twice the enthalpy barrier of the N → bR transition (≈ 100 kJ/mol) and about 150 J/mol K of the entropy change of the activation (compare with data in Table 2). An analogous analysis has been made of the temperature behavior of τ_7 (M ↔ N decay). Therefore, assuming that the energy barriers of all rate-limiting steps that control the relaxation pathway of the bR photocycle do not drastically change, the submodel (M ↔ N) → (N ↔ O) → bR is more realistic.

In Fig. 5 the two solid gray lines represent the nonlinear least-squares fit of temperature dependencies of τ_6 and τ_7, using the formula

$$k_{app} = \frac{kT}{h}\exp\left(\frac{\Delta S^{\#}}{R} - \frac{\Delta E^{\#}}{RT}\right)\Big/1 + \exp\left(-\frac{\Delta S^{eq}}{R} + \frac{\Delta E^{eq}}{RT}\right),$$

i.e., the apparent rate constant is the product of the intrinsic rate and the constant of quasiequilibrium. Of course, for such nonlinear parameters the accuracy of the derived values is much lower than in a linear fit (compare the errors in the Table 2), but, nevertheless, it gave a reasonable estimation of quasiequilibrium constants of (M ↔ N) and (N ↔ O) as ΔS_{NM} = 210 ± 60 J/mol K, ΔE_{NM} = 60 ± 20 kJ/mol and ΔS_{ON} = 160 ± 80 J/mol K, ΔE_{ON} = 50 ± 20 kJ/mol.

In our previous paper (Chizhov et al., 1992a) we used a simpler method to measure ΔS_{ON} and ΔE_{ON}, which, however, contained higher systematic errors because the (M ↔ N) equilibrium was not resolved. Therefore the values derived in that paper appear as a mixture of two quasiequilibria and their accuracy was overestimated. Assuming that the (N ↔ O) is a fast reversible *cis-trans* reisomerization of the protonated Schiff base, a value of ΔS_{ON} about 10 times higher than that of ΔS_{LM} would be reasonable because the reisomerization involves more degrees of freedom than deprotonation.

On the other hand, our analysis shows that the reprotonation of the Schiff base (M ↔ N) involves a large change in entropy. The reason for this is currently unclear. The answer might be hidden in the molecular mechanism of the set of rate-limiting irreversible and spectrally silent transitions of the protein that control the deprotonation (L ↔ M) and reprotonation (M ↔ N) of the Schiff base and reisomerization (N ↔ O) of the retinal. The role of these protein transitions in the bR photocycle should be analyzed in more detail using another method (e.g., Fourier transform infrared spectroscopy).

The energy currency for the irreversibility of these transitions is below the energy of about 60 kJ/mol, which is still present in the K state (Birge, 1990). Assuming that irreversibility of these transitions means that the back reaction of each step is at least 10 times slower than the forward reaction, the drop of energy in a single step would be about $2RT \approx 5$ kJ/mol. The overall cost of five steps is therefore about 25 kJ/mol. Which part of this energy would simply dissipate and which would be channeled into proton transport is the subject of further investigations.

CONCLUSIONS

1. The linear scheme of the bR photocycle derived on the basis of global multiexponential analysis of transient absorbency changes in the visible spectrum at different temperatures at pH 7.2 is sufficient to describe the experiments without the introduction of additional free parameters.

2. This scheme explains why the number of observed kinetic components of the relaxation (at least seven distinct exponents) exceeds the number of spectrally distinct species (K_{600}, L_{540}, M_{410}, N_{560}, and O_{630}). There is no necessity to introduce any additional assumptions (or free parameters) to

overcome this apparent discrepancy. Observed kinetics can be interpreted on the basis of a simple linear sequence of irreversible transitions which, in fact, do not themselves produce distinct spectral changes but control the relative fraction of spectral intermediates that equilibrate between each other faster.

3. According to spectral maxima these quasiequilibria, (L ↔ M), (M ↔ N), and (N ↔ O), correspond, respectively, to the deprotonation, reprotonation, and most probably *cis-trans* reisomerization of a retinal chromophore of the bR.

4. The (L ↔ M) deprotonation of the SB indicates a reversible jump of the proton between the Schiff base nitrogen and primary acceptor group (Asp85), because it does not contain significant enthalpy and entropy changes and, therefore, is almost temperature independent in the range we analyzed. A much more pronounced temperature dependence of the (M ↔ N) quasiequilibrium indicates that additional protein (and/or chromophore) degrees of freedom are involved in the reprotonation of the SB (the N state has about 60 kJ/mol enthalpy and 200 J/mol K entropy more than the M state). The (N ↔ O) quasiequillibrium that corresponds to the reisomerization of retinal has nearly the same features.

5. The interplay (M ↔ N) of a proton between the SB and donor group can be broken if another proton from the cytoplasmic site of the bR arrives at the donor group. This is expected because the slowest apparent half-time of 5 ms, which we assigned to the transition from M ↔ N to N ↔ O, is the most pH-dependent component of the photocycle (Xie et al., 1987).

6. Analysis of temperature dependencies of the observed rate constants shows that conformational protein modes that control proton pumping probably have very similar barriers of enthalpy of activation (about 50 kJ/mol), and the slowing of subsequent steps of relaxation on the path to deprotonation is mainly due to the decrease in the entropic part of the barriers from about +40 to −40 J/mol K. At the higher limit this gives kinetics in the microsecond range and at the lower limit slows the relaxation to milliseconds. On the path of reprotonation of the SB, there are at least two steps (5 ms and 1.5 ms) that have a descending order of half-times. This apparent acceleration of the relaxation might be explained by the opposite trend: an increase in the entropy of activation. In other words, the conformational relaxation of the protein looks more specific in the sense of number of degrees of freedom necessary for the transition controlling the deprotonation, but less specific on the path of reprotonation. The underlying mechanism of this protein function is still unclear.

APPENDIX

Analytical form of irreversible sequence of transitions

We present here the simplest analytical form of the general solution for a sequence of any number of irreversible first-order transitions that must first be applied to the analysis of a multiexponential kinetic problem. The sequence

$$P_1 \xrightarrow{k_1} P_2 \xrightarrow{k_2} \cdots \xrightarrow{k_{i-1}} P_i \xrightarrow{k_i} \cdots \qquad \text{(A)}$$

has the Master equation:

$$\begin{aligned} \dot{P}_1 &= -k_1 P_1 \\ \dot{P}_2 &= -k_2 P_2 + k_1 P_1 \\ &\cdots \\ \dot{P}_i &= -k_i P_i + k_{i-1} P_{i-1}, \\ &\cdots \end{aligned} \qquad (1)$$

which with initial conditions $P_1(0) = 1$, $P_{i>1} = 0$ has the exact solution

$$P_i = \sum_{j=1}^{i} \mathbf{a}_{ij} e^{-k_j t} \qquad (2)$$

where

$$\mathbf{a}_{ij} = \prod_{m=1}^{i-1} k_m \Big/ \prod_{\substack{m=1 \\ m \neq j}}^{i} (k_m - k_j),$$

and $P_i(t)$ is the probability of finding a molecule in the state i at the time t. If the process includes n steps, then there is the $n \times n$ matrix $\mathbf{a}_{ij}$, which has all zero elements above diagonal, i.e., $P_1 = a_{11} e^{-k1t}$, $P_2 = a_{21} e^{-k1t} + a_{22} e^{-k2t}$, and so on. In another words, Eq. 2 states that any state i in the chain (A) includes in its probability value $P_i(t)$ information about all preceding steps and the first following step ($j = 1 \cdots i$), i.e., the state $P_i(t)$ "remembers" all of the past and "knows" only the nearest future. This is a direct consequence of the irreversibility of transitions.

In an experiment one can find n exponential components of relaxation, i.e.,

$$B(\lambda, t) = \sum_{i=1}^{n} b_i(\lambda) e^{-k_i^* t}, \qquad (3)$$

where $b_i(\lambda)$ are spectra of corresponding exponential components k_i^*.

If $b_i(\lambda)$ spectra are differential absorbencies with respect to the final state (and/or state before excitation), then

$$B(\lambda, t) = \sum_{i=1}^{n} b_i(\lambda) e^{-k_i^* t} = F_c \sum_{i=1}^{n} \Delta\epsilon_i(\lambda) P_i(t), \qquad (4)$$

where the cycling fraction $F_c = N_c/N_0$ (i.e., the fraction of molecules that after excitation comes to the state P_1) and differential spectra $\Delta\epsilon_i(\lambda) = \epsilon_i - \epsilon_0$ (where ϵ_i is the absolute spectra of state P_i, and ϵ_0 is the absolute spectra of ground state). Substitution of $P_j(t)$ from Eq. 2 and assignment of experimentally observed k_i^* to intrinsic k_i (for instance, assuming a descending order of transitions $k_i < k_{i-1}$) would give the opportunity to calculate the matrix $\mathbf{a}_{ij}$ that has a simple triangle form. Then the problem of deriving the spectra of intermediates is only dependent upon the single unknown parameter F_c:

$$b_i(\lambda) = F_c \sum_{j=i}^{n} \mathbf{a}_{ji} \Delta\epsilon_j(\lambda). \qquad (5)$$

Equation 5 matches a trend opposite that of Eq. 2: each spectral amplitude b_i includes the spectra of P_i as well as the spectra of all following states

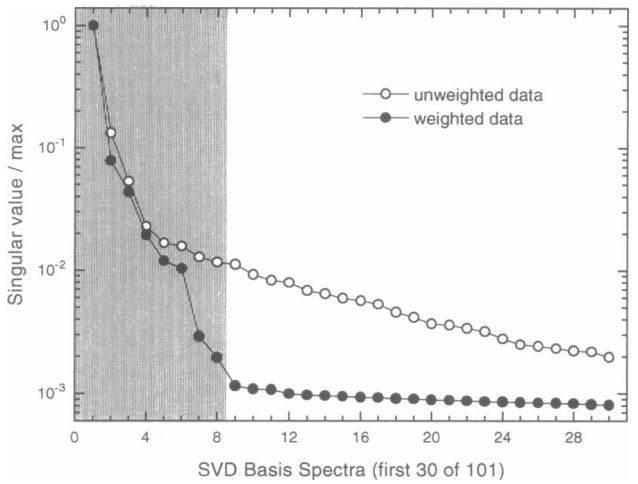

FIGURE 11 Normalized singular values of basis spectra of the SVD analysis of weighted and unweighted transient spectral kinetic data of the bR photocycle at 8°C.

until the end of process ($j = i \cdots n$). Therefore, it is easy to calculate recursively all spectra $\Delta\epsilon_i(\lambda)$ from the spectra of exponents $b_i(\lambda)$ starting from the last state n:

$$\Delta\epsilon_i(\lambda) = (b_i(\lambda) - \sum_{j=i+1}^{n} \mathbf{a}_{ij}\Delta\epsilon_j(\lambda))/\mathbf{a}_{ii}F_c. \qquad (6)$$

Any single reassignment of intrinsic rate constants to observed rate constants when at some step $k_i > k_{i-1}$ (e.g., state P_i decays faster than it forms) would crucially change the spectra of P_i, would interfere much less with the later states (if they remain in descending order), and would not affect the spectra of former states at all. This is illustrated in submodels A and B of Fig. 9.

It is easy to show also that the transition between two spectrally identical states (i.e., $\Delta\epsilon_i = \Delta\epsilon_{i+1}$) can give principally nonzero amplitude in the apparent kinetics. Physically this would mean that such a spectrally silent transition does not even change a probable quasiequilibrium of states (if $\Delta\epsilon_i$ shows this feature), but occurs as a rate-limiting step.

A further complication of the relaxation scheme might contain two distinct possibilities: branching and/or reversibility. It can be shown that introducing a branching would not break the validity of Eq. 2, but after branching would split the F_c into additional unknowns, $F_c = F_c^1 + F_c^2$. Reversibility will complicate the problem crucially: there will be no direct conformity of experimentally observed n rate constants k_i^* to intrinsic ones (that can be in principle as much as $n(n-1)$), but k_i^* will be eigenvalues of the matrix of internal rates of the corresponding Master equation. This most general case has been analyzed by Nagle (1991).

On singular value decomposition

The singular value decomposition (SVD) method as a special data filter may help to determine the number of significant components that participate in the relaxation. Basis spectra and their time courses might be then used as a reduced data base for the global multiexponential analysis (Henry and Hofrichter, 1992). Basis spectra have no physical meaning, but the derived apparent rate constants of the nonlinear multiexponential fit of time courses must be invariant and describe as well nonfiltered apparent spectral kinetics. Therefore the real meaning of this procedure is the ability to apply the nonlinear simultaneous multiexponential fit of apparent rate constants on a few time courses but not on all measured wavelengths and, therefore, considerably reduce the computational time. On the other hand, any filtering of experimental data might carry the risk of missing some significant kinetic components that would contribute to the "noisy" basis spectra and therefore might be withdrawn from the beginning.

To check the reliability of the SVD method we applied this tool (the IDL subroutine on the SUN computer) to our data. In Fig. 11 normalized singular values of the first 30 (from 101) basis spectra of SVD are shown on a log scale. Open circles correspond to the SVD of an unweighted data set (8°C, 101 wavelength × 400 log time points), and filled circles are the results of SVD of the same but weighted data set (see Computational Methods). As seen in Fig. 11, only properly weighted data give the striking difference in singular values between basis spectra that contain information and those that SVD arranges from the noise of the data. The number of informative basis spectra of the SVD of weighted data (eight) is in excellent agreement with the number of significant components of relaxation that we found independently from direct multiexponential analysis.

We thank M. Geeves and R. S. Goody for helpful discussions.

REFERENCES

Alexiev, U., R. Mollaaghabada, P. Scherrer, H. G. Korana, and M. P. Heyn. 1995. Rapid long-range proton diffusion along the surface of the purple membrane and delayed proton transfer into the bulk. *Proc. Natl. Acad. Sci. USA.* 92:372–376.

Becher, B. and J. Y. Cassim. 1976. Effects of light adaptation on the purple membrane structure of *Halobacterium halobium. Biophys. J.* 16: 1183–1200.

Birge, R. R. 1990. Nature of the primary photochemical events in rhodopsin and bacteriorhodopsin. *Biochim. Biophys. Acta.* 1016:293–327.

Cao, Y., L. S. Brown, J. Sasaki, A. Maeda, R. Needleman, and J. K. Lanyi. 1995. Relationship of proton release at the extracellular surface to deprotonation of the Schiff base in the bacteriorhodopsin photocycle. *Biophys. J.* 68:1518–1530.

Chance, B., M. Porte, B. Hess, and D. Oesterhelt. 1975. Low temperature kinetics of H^+ changes of bacterial rhodopsin. *Biophys. J.* 15:913–917.

Chernavskii, D. S., I. V. Chizhov, R. H. Lozier, T. M. Murina, A. M. Prokhorov, and B. V. Zubov. 1989. Kinetic model of bacteriorhodopsin photocycle: pathway from M state to bR. *Photochem. Photobiol.* 49: 649–653.

Chizhov, I., M. Engelhard, D. S. Chernavskii, B. Zubov, and B. Hess. 1992a. Temperature and pH sensitivity of the O_{640} intermediate of the bacteriorhodopsin photocycle. *Biophys. J.* 61:1001–1006.

Chizhov, I., M. Engelhard, A. V. Sharkov, and B. Hess. 1992b. Two quantum absorption of ultrashort laser pulses by the bacteriorhodopsin chromophore. *In* Structure and Functions of Retinal Proteins. J. L. Rigaud, editor. John Libbey and Co., London. 171–173.

Chu Kung, M., D. Devault, B. Hess, and D. Oesterhelt. 1975. Photolysis of bacterial rhodopsin. *Biophys. J.* 15:907–911.

Druckmann, S., M. P. Heyn, J. K. Lanyi, M. Ottolenghi, and L. Zimanyi. 1993. Thermal equilibration between the M and N intermediates in the photocycle of bacteriorhodopsin. *Biophys. J.* 65:1231–1234.

Gillbro, T. 1978. Flash kinetic study of the last steps in the photoinduced reaction cycle of bacteriorhodopsin. *Biochim. Biophys. Acta.* 504: 175–186.

Heberle, J., D. Oesterhelt, and N. A. Dencher. 1993. Decoupling of photo- and proton cycle in the Asp85 → Glu mutant of bacteriorhodopsin. *EMBO J.* 12:3721–3727.

Henry, E. R., and J. Hofrichter. 1992. Singular value decomposition: application to analysis of experimental data. *Methods Enzymol.* 210: 129–192.

Hofrichter, J., E. R. Henry, and R. H. Lozier. 1989. Photocycles of bacteriorhodopsin in light- and dark-adapted purple membrane studied by time-resolved absorption spectroscopy. *Biophys. J.* 56:693–706.

Imamoto, Y., Y. Shichida, J. Hirayama, H. Tomioka, N. Kamo, and T. Yoshizawa. 1992. Nanosecond laser photolysis of phoborhodopsin from Natronobacterium pharaonis: appearance of KL and L intermediates in

the photocycle at room temperature. *Photochem. Photobiol.* 56: 1129–1134.

Korenstein, R., B. Hess, and D. Kuschmitz. 1978. Branching reactions in the photocycle of bacteriorhodopsin. *FEBS Lett.* 93:266–270.

Lanyi, J. K. 1993. Proton translocation mechanism and energetics in the light-driven pump bacteriorhodopsin. *Biochim. Biophys. Acta.* 1183: 241–261.

Lozier, R. H., R. A. Bogomolni, and W. Stoeckenius. 1975. Bacteriorhodopsin: a light-driven proton pump in *Halobacterium halobium. Biophys. J.* 15:955–962.

Metzler, D. E., and C. M. Harris. 1978. Shapes of spectral bands in visual pigment. *Vision Res.* 18:1417–1420.

Milder, S. J., T. E. Thorgeirsson, L. J. W. Miercke, R. M. Stroud, and D. S. Kliger. 1991. Effects of detergent environments on the photocycle of purified monomeric bacteriorhodopsin. *Biochemistry.* 30:1751–1761.

Müller, K.-H., H. J. Butt, E. Bamberg, K. Fendler, B. Hess, F. Siebert, and M. Engelhard. 1991. The reaction cycle of bacteriorhodopsin: an analysis using visible absorption, photocurrent and infrared techniques. *Eur. Biophys. J.* 19:241–251.

Müller, K.-H., and T. Plesser. 1991. Variance reduction by simultaneous multi-exponential analysis of data sets from different experiments. *Eur. Biophys. J.* 19:231–240.

Nagle, J. F. 1991. Solving complex photocycle kinetcs. Theory and direct method. *Biophys. J.* 59:476–487.

Nagle, J. F., L. Zimanyi, and J. K. Lanyi. 1995. Testing BR photocycle kinetics. *Biophys. J.* 68:1490–1499.

Oesterhelt, D. and W. Stoeckenius. 1974. Isolation of the cell membrane of *Halobacterium halobium* and its fractionation into red and purple membrane. *Methods Enzymol.* 31:667–678.

Oesterhelt, D., J. Tittor, and E. Bamberg. 1992. A unifying concept for ion translocation by retinal proteins. *J. Bioenerg. Biomembr.* 24:181–191.

Parodi, L. A., R. H. Lozier, S. M. Bhattacharjee, and J. F. Nagle. 1984. Testing kinetic models for the bacteriorhodopsin photocycle. II. Inclusion of an O to M back-reaction. *Photochem. Photobiol.* 40:501–512.

Sherman, W. V., R. Korenstein, and S. R. Caplan. 1976. Energetics and chronology of phototransients in the light response of the purple membrane of *Halobacterium H*; Arrhenius parameters; isotope effects; phase transition photocycle. *Biochim. Biophys. Acta.* 430:454–458.

Váró, G., and J. K. Lanyi. 1991a. Kinetic and spectroscopic evidence for an irreversible step between deprotonation and reprotonation of the Schiff base in the bacteriorhodopsin photocycle. *Biochemistry.* 30: 5008–5015.

Váró, G., and J. K. Lanyi. 1991b. Thermodynamics and energy coupling in the bacteriorhodopsin photocycle. *Biochemistry.* 30:5016–5022.

Xie, A. H., J. F. Nagle, and R. H. Lozier. 1987. Flash spectroscopy of purple membrane. *Biophys. J.* 51:627–635.

Zimanyi, L., G. Váró, M. Chang, B. Ni, R. Needleman, and J. K. Lanyi. 1992. Pathways of proton release in the bacteriorhodopsin photocycle. *Biochemistry.* 31:8535–8543.

Zubov, B. V., N. A. Sulimov, N. M. Chernavskaya, D. S. Chernavsky, and I. V. Chizhov. 1982. Kinetics of photocycle primary stages of bacteriorhodopsin at low temperatures. *Biofizika (USSR).* 27:357–361.